

# Diffraction waves on large aspect ratio rectangular submerged breakwaters

Esmael Masoudi<sup>a,\*</sup>, Lian Gan<sup>a</sup>

<sup>a</sup>*Department of Engineering, Durham University, United Kingdom*

---

## Abstract

In this paper, hydrodynamic characteristics of two-dimensional submerged breakwaters in water of finite depth and infinite domain interacting with sinusoidal waves are studied from both analytical and numerical approaches. Added mass and damping coefficients are obtained following the determination of radiation potentials in three degrees of freedom (sway, heave and roll). Diffraction problem is then solved according to the linear wave theory and the resulting forces are derived. To verify the results, a comparison of the solution from the analytical method with those obtained by the boundary element method is made and a good agreement is observed. Additionally, high aspect ratio horizontal and vertical flat submerged breakwaters are proposed and their hydrodynamic characteristics are analyzed using the numerical and analytical methods. Results show that the horizontal flat submerged breakwater generates low transmitted waves. However, the vertical flat submerged breakwater transmits almost the entire incident wave energy. A parametric study on the effect of submergence depth and the width of the structure on the maximum diffraction wave amplitude, which is responsible for the transmitted wave energy, is carried out and a better understanding of the variation of diffraction wave amplitudes with respect to dominant parameters and wave frequency is achieved.

---

## 1. Introduction

The development of coastal or inland waters may often depend on sea behaviour at a specific site. Breakwaters of various dimensions and configurations have been widely employed to increase the use of locations exposed to wave attack. The main purpose of installing a breakwater is to reduce wave height to an acceptable level with respect to usage of the site. The increase in the number of private pleasure crafts and small vessels has engendered a demand for more sheltered sites. Affordability and required level of wave protection would often dictate possible breakwater alternatives. Rubble mound breakwaters have been widely used to attenuate surface water waves. In

recent years, several floating breakwaters (FBs) are employed in coastal areas all over the world. Submerged breakwaters (SBs) were also a field of interest to many researchers. FBs and SBs usually consist of a floating pontoon with finite draft which are exposed to hydraulic waves. Motions of these breakwaters are usually constrained to three degrees of freedom. That is sway, heave and roll.

In the framework of numerical methods to study breakwater's performance in waves, finite element method (FEM) and boundary element method (BEM) are two popular and effective approaches which have been widely applied to breakwater performance analysis. As far as FEM and BEM are concerned, there are many published studies. As examples, Yamamoto et al. (1980) used BEM to solve two-dimensional problems of the response of the moored floating objects to water waves. They solved the boundary value prob-

---

\*Corresponding author

*Email addresses:* [esmaeel.masoudi@durham.ac.uk](mailto:esmaeel.masoudi@durham.ac.uk) (Esmael Masoudi), [lian.gan@durham.ac.uk](mailto:lian.gan@durham.ac.uk) (Lian Gan)

35 lem numerically by direct use of Green's identity  
36 formula for a potential function. Their results  
37 mostly focused on mooring configuration effects  
38 on wave attenuation characteristic of the float-  
39 ing body. Li et al. (1991) employed finite - in-  
40 finite element method to obtain hydrodynamic  
41 exciting forces in regular waves. They utilized  
42 the inhomogeneous far field boundary conditions  
43 and the higher order asymptotic solutions to ob-  
44 tain second order diffraction forces and wave run-  
45 up profiles on a vertical cylinder. Their method  
46 showed better agreement with experimental re-  
47 sults compared to the predictions from the lin-  
48 ear theory. Sannasiraj et al. (1995) applied FEM  
49 to investigate the radiation and diffraction prob-  
50 lem of a horizontal FB under the action of multi-  
51 directional waves. They evaluated wave exciting  
52 forces and relative induced responses using linear  
53 transfer-function approach for a rectangular cross  
54 section floating structure. The force and response  
55 ratio were also obtained in their study for fre-  
56 quency dependent-independent cosine power type  
57 directional spreading functions. Sannasiraj et al.  
58 (2001) also used the same finite element tech-  
59 nique to study multiple floating structures. Wu  
60 and Taylor (2003) used coupled FEM and BEM,  
61 based on the combination of their strengths, to  
62 study nonlinear interactions between waves and  
63 bodies. They introduced auxiliary functions to  
64 decouple the mutual dependence of the body ac-  
65 celeration and hydrodynamic forces. Present-  
66 ing their results for submerged circular and el-  
67 liptical cylinder, they asserted that their numer-  
68 ical scheme could also be used for floating struc-  
69 tures. Kunisu (2010) compared the results of  
70 BEM with those from experiments and studied  
71 the wave forces on a submerged floating tunnel.  
72 Evaluating exciting forces on a submerged circu-  
73 lar cylinder using BEM as well as the well-known  
74 Morison's equation, they concluded that the in-  
75 ertia forces are dominant in large circular cylin-  
76 ders only when the Keulegan-Carpenter number  
77 is less than 15 for all incident wave frequencies.  
78 Chen et al. (2016) built FEM based Navier-Stokes  
79 equation and volume of fluid (VOF) method  
80 to investigate wave energy extraction by two-  
81 dimensional oscillating cylinders in linear waves

for incompressible viscous flows. Based on wave  
climate off China's shore and building cost, they  
suggested that the cylinder diameter must be  
twice the incident wave height in order to obtain  
the best energy harvest efficiency. Zhan et al.  
(2017) applied zonal hybrid Reynolds averaged  
Navier-Stokes (RANS)/laminar method with a  
new meshing strategy to investigate hydrody-  
namic performance of an inverse T-type break-  
water. They investigated heave and pitch trans-  
fer functions as well as transmission and reflec-  
tion coefficients for floating and fixed breakwa-  
ters in regular and irregular waves. Tabatabaei  
and Zeraatgar (2018) utilized FEM for studying  
a moored pontoon type FB considering response  
amplitude operators (RAOs). They suggested  
that in spite of the fact that rectangular FBs are  
more commonly used in industry, circular FBs  
should also be considered for their better hydro-  
dynamic performance in a wider range of incident  
wave frequencies. Masoudi (2019) employed BEM  
to study inverse T-type FB's hydrodynamic per-  
formance in sinusoidal waves. It was concluded  
that inverse T-type FB has lower transmission co-  
efficient than rectangular FB over a wide range of  
incident wave frequencies and so could be consid-  
ered for practical applications.

Analytical methods have also been used in  
many studies, some of which are mentioned next.  
Garrett (1970) discussed about the excitation of  
waves inside a partially immersed open circular  
cylinder. He considered incident plane wave ex-  
panded in Bessel functions and for each mode  
he formulated the problem in terms of the ra-  
dial displacement on the cylindrical interface be-  
low the cylinder. He deduced that the phase of  
the solution is independent of depth and reso-  
nances are found at wave-numbers close to those  
of free oscillations in a cylinder extending to the  
bottom. Garrett (1971) also discussed scattering  
gravity waves by a circular cylinder in order to  
determine the horizontal and vertical forces as  
well as torques on a dock. He discussed that  
the phase of the solution is independent of depth  
and so may be obtained from an infinite set of  
real equations, which were solved numerically by  
Galerkin's method. Hulme (1982) derived added

129 mass and damping coefficients and wave force act- 176  
130 ing on a floating hemisphere oscillating in incom- 177  
131 pressible inviscid fluid. Wu and Taylor (1990) and 178  
132 Wu (1993) solved second order diffraction and ra- 179  
133 diation problems for a horizontal cylinder in finite 180  
134 water depth. They stated that for horizontal os- 181  
135 cillation motion of the cylinder, the first-order po- 182  
136 tential is asymmetric but the second-order poten- 183  
137 tial is symmetric. Berggren and Johansson (1992) 184  
138 presented hydrodynamic coefficients of a wave en- 185  
139 ergy device consisting of a buoy connected to a 186  
140 submerged plate. Lee (1995) studied the heave 187  
141 radiation problem of a rectangular structure in 188  
142 which non-homogeneous boundary value problem 189  
143 is linearly decomposed into a homogeneous one. 190  
144 They showed that the presented solution satisfac- 191  
145 es the non-homogeneous boundary condition in a 192  
146 sense of series convergence. They also found that 193  
147 smaller structure submergence and larger struc- 194  
148 ture width would result in larger waves, radia- 195  
149 tion added mass and damping coefficients. Hsu 196  
150 and Wu (1997) compared BEM with their analy- 197  
151 tical method for analyzing hydrodynamic co- 198  
152 efficients of an oscillating rectangular structure 199  
153 with a side wall and concluded that the reso- 200  
154 nant behavior would appear when the clearance 201  
155 between the sidewall and the structure equals 202  
156 integer times of half wave length generated by 203  
157 the oscillating structure. Abul-Azm and Gesraha 204  
158 (2000) used an eigen-function expansion method 205  
159 to study a moored FB in oblique waves. They 206  
160 deduced that hydrodynamic performance of the 207  
161 pontoon type FB in wave reflection or transmis- 208  
162 sion has a strong dependence on the relative di- 209  
163 mension of the cross section, while dynamic prop- 210  
164 erties mostly depend on inertial characteristic. 211  
165 Williams et al. (2000) proposed an appropriate 212  
166 Green's function to study hydrodynamic proper- 213  
167 ties of a pair of long floating pontoon breakwaters 214  
168 of rectangular section restrained by linear sym- 215  
169 metric moorings. They showed that wave reflec- 216  
170 tion properties of twin pontoons depend strongly 217  
171 on their width, draft and spacing and the moor- 218  
172 ing line stiffness, while their excess buoyancy is 219  
173 of less importance. Zheng et al. (2004a,b) derived 220  
174 an analytical solution for radiation and diffraction 221  
175 problem of a rectangular buoy and presented ex-

tensive results from added mass and damping co- 176  
efficients and the effect of sidewall. Masoudi and 177  
Zeraatgar (2016) employed the method of separa- 178  
tion of variables, including eigen-function expan- 179  
sion method, in which radiation and diffraction 180  
problem is solved in three sub-domains in order 181  
to study hydrodynamic characteristics, such as 182  
added mass and damping coefficients as well as ex- 183  
citing forces, of a two-dimensional rectangular FB 184  
in water of finite depth and infinite domain. Deng 185  
et al. (2019) used a semi-analytical method to 186  
study hydrodynamic performance of a T-type FB. 187  
The effects of the height and setup position of ver- 188  
tical screen on the dynamic response and hydro- 189  
dynamic characteristics of the breakwater are dis- 190  
cussed. Mohapatra and Soares (2019) derived the 191  
three-dimensional Green's function and Fourier- 192  
type expansion formula for analyzing wave reflec- 193  
tion by a rigid vertical wall with a floating and 194  
submerged elastic plate. They used linear struc- 195  
tural response and thin plate theory to obtain hy- 196  
droelastic response of the structure and concluded 197  
that mitigation of hydroelastic response of float- 198  
ing structures depends significantly on modes of 199  
oscillation, mooring stiffness, compressive force, 200  
rigidity and suitable positioning of the submerged 201  
horizontal flexible membrane. 202

Analytical solution is normally approached by 203  
dividing the whole domain to sub-domains and 204  
then approximating the velocity potentials in each 205  
sub-domain using orthogonal functions. After the 206  
boundary conditions are satisfied on the whole 207  
domain and on the common boundaries between 208  
sub-domains, the unknown coefficients in orthog- 209  
onal functions are solved and the velocity poten- 210  
tials become explicit in sub-domains. Having de- 211  
termined the velocity potentials and wave char- 212  
acteristics on both sides of the breakwater body, 213  
the transmission and reflection coefficients are ob- 214  
tained. Although assumptions are usually in- 215  
volved for simplification reasons, the results are 216  
explicit. 217

High aspect ratio SBs which could be made 218  
by a simple flat thin plate of steel are expected to 219  
be good substitutes for other conventional type 220  
of breakwaters having larger volume of materials. 221  
The former could be moored using typical moor- 222

ings such as catenary lines by adding buoyancy  
aids to the structure. In this study, two types  
of two-dimensional rectangular high-aspect ratio  
flat SBs (horizontally and vertically) submerged  
in water of finite depth and infinite extent sub-  
jected to regular sinusoidal waves are analytically  
studied by solving the velocity potential equations  
using the separation of variables method. Similar  
to other analytical approaches, turbulence effect  
are neglected. The method of separation of vari-  
ables is firstly verified by a typical conventional  
SB geometry Zheng et al. (2007). Additionally,  
BEM using ANSYS AQWA software is employed  
to solve diffraction and radiation problems for  
comparison. Next, hydrodynamic characteristics,  
including exciting forces as well as the reflection  
and transmission coefficients are analyzed. In par-  
ticular, a parametric study on the main param-  
eters e.g. submergence depth and the width of the  
breakwater are carried out in order to estimate  
their effects on the diffraction wave amplitude,  
which is a dominant parameter of the transmis-  
sion coefficient. Finally, the establishment of the  
diffraction wave is discussed and its effect on hy-  
drodynamic performance is concluded.

## 2. Method

For large breakwater length to the wavelength  
ratios, fluid is assumed to be incompressible, in-  
viscid and irrotational. As such, the velocity po-  
tential  $\phi$  satisfies the Laplace equation as shown  
in Equation (1). The velocity components and  
pressure can then be expressed by Equation (2)  
and Equation (3), respectively.

$$\nabla^2 \phi = 0 \quad (1)$$

$$\frac{\partial \phi}{\partial x} = u, \quad \frac{\partial \phi}{\partial y} = v, \quad \frac{\partial \phi}{\partial z} = w \quad (2)$$

$$\frac{\partial \phi}{\partial t} + \frac{1}{2} \nabla \phi^2 + gz + \frac{P}{\rho} = 0, \quad (3)$$

where  $u$ ,  $v$  and  $w$  are velocity components in  $x$ ,  $y$   
and  $z$  direction respectively.  $P$  is the dynamic  
pressure,  $\rho$  is water density and  $g$  is the gravita-  
tional acceleration. Basic problem configuration

of the breakwater and the coordinate system are  
shown in Figure 1. It is assumed that a linear  
wave with amplitude  $A_i$  and angular frequency  
 $\omega = 2\pi/T_i$  propagates in a direction at an angle  $\theta$   
to the  $+x$  axis. The total potential  $\phi$  is composed  
of incident wave potential  $\phi_i$ , diffraction poten-  
tial  $\phi_d$ , and radiation potentials  $\phi_r$ . The incident  
wave potential for a regular sinusoidal wave can be  
written as  $\phi_i = \varphi_i(x, z) \exp(jky \sin \theta)$ , in which:

$$\varphi_i = -\frac{jgA_i \cosh[k(z + h_1)]}{\omega \cosh(kh_1)} \exp(jkx \cos \theta) \quad (4)$$

where  $k$  is the wave number,  $j$  represents unit  
imaginary number and  $h_1$  is the depth of water.  
Also

$$\omega^2 = gk \tanh(kh_1) \quad (5)$$

is known as the *dispersion equation*. The diffrac-  
tion potential  $\phi_d$  is induced by the interaction of  
incident wave and the breakwater. The induced  
potential from the motions of structure in three  
degrees of freedom are known as radiation poten-  
tial  $\phi_r$ .

Referring to Figure 1, the problem is consid-  
ered as two-dimensional. That is, motions are re-  
stricted in heave, sway and roll, denoted as indices  
1, 2 and 3, respectively. Hence the total potential  
 $\phi_t$  could be expressed as:

$$\phi_t = \phi_i + \phi_d + \sum_{L=1}^3 \phi_r^L \quad (6)$$

where  $L$  refers to the assigned motion number and  
 $\phi_r^L$  is the radiation potential of the  $L^{th}$  motion.  
The unknown terms in the above equation are  $\phi_d$   
and  $\phi_r^L$  which will be addressed next.

*The diffraction term  $\phi_d$*

The linear diffraction term and its boundary  
conditions can be expressed by the oscillatory  
function

$$\phi_d(x, z, y) = \varphi_d(x, z) \exp(jky \sin \theta) \quad (7)$$

$$\frac{\partial \varphi_d}{\partial z} - \frac{\omega^2}{g} \varphi_d = 0 \quad (z = 0) \quad (8)$$



velocity potentials are given from Equation (19) to Equation (22) for regions I to IV, respectively.

$$\varphi_{d_1} = \sum_{n=1}^{\infty} A'_{1n} e^{-\gamma_n(x-b)} \cos[\lambda_n (z + h_1)] \quad (19)$$

$$\begin{aligned} \varphi_{d_2} = -\varphi_i + \sum_{n=1}^{\infty} [A'_{2n} e^{\mu_n(x+b)} \\ + B'_{2n} e^{-\mu_n(x-b)}] \cos[\beta_n (z + h_1)] \quad (20) \end{aligned}$$

$$\varphi_{d_3} = \sum_{n=1}^{\infty} A'_{3n} e^{\gamma_n(x+b)} \cos[\lambda_n (z + h_1)] \quad (21)$$

$$\begin{aligned} \varphi_{d_4} = -\varphi_i + \sum_{n=1}^{\infty} [A'_{4n} e^{v_n(x+b)} \\ + B'_{4n} e^{-v_n(x-b)}] \cos[\alpha_n (z + s_1)] \quad (22) \end{aligned}$$

For the radiation term, velocity potentials are given from Equation (23) to Equation (26) for regions I to IV, respectively.

$$\varphi_{r_1}^L = \sum_{n=1}^{\infty} A_{1n}^L e^{-\gamma_n(x-b)} \cos[\lambda_n (z + h_1)] \quad (23)$$

$$\begin{aligned} \varphi_{r_2}^L = \varphi_{r_{2p}}^L + \sum_{n=1}^{\infty} [A_{2n}^L e^{\mu_n(x+b)} + \\ B_{2n}^L e^{-\mu_n(x-b)}] \cos[\beta_n (z + h_1)] \quad (24) \end{aligned}$$

$$\varphi_{r_3}^L = \sum_{n=1}^{\infty} A_{3n}^L e^{\gamma_n(x+b)} \cos[\lambda_n (z + h_1)] \quad (25)$$

$$\begin{aligned} \varphi_{r_4}^L = \varphi_{r_{4p}}^L + \sum_{n=1}^{\infty} [A_{4n}^L e^{v_n(x+b)} + \\ B_{4n}^L e^{-v_n(x-b)}] \cos[\alpha_n (z + s_1)] \quad (26) \end{aligned}$$

In the equations above, eigenvalues  $(\gamma_n, \mu_n, \beta_n, \lambda_n, v_n, \alpha_n)$  are given by:

$$\lambda_1 = -jk, \quad k \tanh(kh_1) = \frac{\omega^2}{g} \quad n = 1 \quad (27)$$

$$\lambda_n \tan(\lambda_n h_1) = -\frac{\omega^2}{g} \quad n = 2, 3, \dots \quad (28)$$

$$\alpha_1 = -jk_1, \quad k_1 \tanh(k_1 s_1) = \frac{\omega^2}{g} \quad n = 1 \quad (29)$$

$$\alpha_n \tan(\alpha_n s_1) = -\frac{\omega^2}{g} \quad n = 2, 3, \dots \quad (30)$$

$$\beta_n = \frac{(n-1)\pi}{h_1 - d} \quad n = 1, 2, 3, \dots \quad (31)$$

$$v_n = \begin{cases} -j\sqrt{k_1^2 - k_0^2} & n = 1 \\ \sqrt{\alpha_n^2 + k_0^2} & n = 2, 3, \dots \end{cases} \quad (32)$$

$$\gamma_n = \begin{cases} jk \cos \theta & n = 1 \\ \sqrt{\lambda_n^2 + k_0^2} & n = 2, 3, \dots \end{cases} \quad (33)$$

$$\mu_n = \begin{cases} k_0 & n = 1 \\ \sqrt{\beta_n^2 + k_0^2} & n = 2, 3, \dots \end{cases} \quad (34)$$

Furthermore, in Equation (24) and Equation (26),  $\varphi_{r_{2p}}^L$  and  $\varphi_{r_{4p}}^L$  are particular solutions for the  $L^{th}$  radiation motion in sub-domain II and IV, respectively, which are given by Zheng et al. (2007) as follows.

$$\varphi_{r_{2p}}^L = C_{F2}(z) [\delta_{1,L} - (x - x_0)\delta_{3,L}] \quad (35)$$

$$\varphi_{r_{4p}}^L = C_{F4}(z) [\delta_{1,L} - (x - x_0)\delta_{3,L}] \quad (36)$$

where:

$$C_{F2}(z) = \frac{\cosh[\mu_1 (z + h_1)]}{\mu_1 \sinh(\mu_1 h_2)} \quad (37)$$

$$C_{F4}(z) = \frac{\frac{\omega^2}{g} \sinh(k_0 z) + k_0 \cosh(k_0 z)}{k_0 \frac{\omega^2}{g} \cosh(k_0 s_1) - k_0 \sinh(k_0 s_1)} \quad (38)$$

The potentials given from Equation (19) to Equation (26) describe the fluid in each region and satisfy all boundary conditions except the common boundaries between the regions. Now, the problem is to evaluate unknown coefficients  $A_{1n}^L, A_{2n}^L, A_{3n}^L, A_{4n}^L, B_{2n}^L, B_{4n}^L$  for the radiation term and  $A_{1n}', A_{2n}', A_{3n}', A_{4n}', B_{2n}', B_{4n}'$  for the diffraction term in the series. It should be noted that each coefficient has a unit which depends on the respective motion in the radiation term. These coefficients are found by imposing the boundary conditions that are the pressure continuity and normal velocity at the common boundaries between the regions, which are  $x = \pm a$  and  $0 < z < -s_1, -s_1 < z < -d_1$  and  $-d_1 < z < -h_1$ . In mathematical terms, it means that potentials and their normal derivatives are equal at boundaries. Satisfying these boundary conditions form a system of 6 linear equations which need to be solved simultaneously. To solve these equations, the orthogonal functions must be truncated. If  $n$  is truncated to  $N$  from Equation (19) to Equation (26), imposing the boundary conditions in the common boundaries will lead to a system of  $6 \times N$  linear equations and equal number of unknown coefficients. Organizing these coefficients in matrices gives

$$S \cdot X = F \quad (39)$$

in which  $X$  is the unknown coefficient matrix. There are three radiation and one diffraction potentials included in Equation (39). It should be noted that  $S$  is a  $6N \times 6N$  matrix which is obtained from satisfying the boundary conditions from Equation (8) to Equation (11) for diffraction and from Equation (13) to Equation (17) for radiation term.  $F$  is a  $1 \times 6N$  matrix which is obtained from satisfying the common boundary conditions between the regions and  $X$  is a  $M \times 6N$  matrix, in which  $M$  is the total number of wave frequencies to solve according to the range and

frequency increments. The detail of this method, including the calculation of  $F$  is discussed in Masoudi and Zeraatgar (2016). Having known  $F$  and  $S$ ,  $X$  is obtained for each of the four potentials. Finally, imposing the coefficients in Equation (19) to Equation (26), the velocity potentials for each region will be obtained.

### Expressions for Hydrodynamic Coefficients and Wave Forces

If we denote the wave force perpendicular to the incident wave as  $F_{w_u}$ , which is independent of  $y$  and time, it can be calculated from the incident and diffracted wave potentials as

$$F_{w_u} = \rho j \omega \int_{S_0} (\varphi_d + \varphi_i) n_u ds \quad (40)$$

in which  $n_u$  is the generalized inward normal to the structure in  $x-z$  plane with  $n_1 = n_z, n_2 = n_x$  and  $n_3 = (z - z_0)n_x - (x - x_0)n_z$  with  $n_x$  and  $n_z$  being the unit inward normal to the surface of the body. Also,  $CF_u$  is the exciting force coefficient which is a non-dimensional form of  $F_{w_u}$  given by:

$$CF_u = \begin{cases} \frac{|F_{w_u}|}{2\rho b d A_i} & u = 1, 2 \\ \frac{|F_{w_u}|}{2\rho b^3 d A_i} & u = 3 \end{cases} \quad (41)$$

The hydrodynamic coefficients including the added mass coefficient  $m_{L,u}$  and the damping coefficient  $N_{L,u}$  are defined by

$$m_{L,u} = \rho \int_{S_0} \text{Re}(\varphi_r^L) n_u ds \quad (42)$$

$$N_{L,u} = \rho \int_{S_0} \text{Im}(\varphi_r^L) n_u ds \quad (43)$$

Also,  $C_{m_u}$  and  $C_{d_u}$  are the non-dimensional added mass and damping coefficients.

$$C_{m_u} = \begin{cases} \frac{m_{u,u}}{2\rho b d} & u = 1, 2 \\ \frac{m_{u,u}}{2\rho b^3 d} & u = 3 \end{cases} \quad (44)$$

$$C_{d_u} = \begin{cases} \frac{N_{u,u}}{2\rho \omega b d} & u = 1, 2 \\ \frac{N_{u,u}}{2\rho \omega b^3 d} & u = 3 \end{cases} \quad (45)$$

Transmission coefficient ( $T_w$ ) is defined as the amplitude of the transmitted wave to the amplitude of the incident wave. Reflection coefficient ( $R_w$ ) is defined as the amplitude of the reflected wave to the amplitude of the incident wave. If breakwaters are assumed to be stationary, using linearised Bernoulli equation, Zheng et al. (2007) obtained transmission and reflection coefficients

$$T_w = \left| \frac{j\omega A'_{31} \cosh(kh_1)}{gA_i} \right| \quad (46)$$

$$R_w = \left| 1 + \frac{j\omega A'_{11} \cosh(kh_1)}{gA_i \exp(jkb \cos \theta)} \right| \quad (47)$$

Longuet-Higgins (1977) proposed the horizontal drift force ( $F_d$ ) in terms of the reflection coefficient as

$$F_d = \left( \frac{Ec_g}{c} \right) (1 + R_w^2 - T_w^2) = \left( \frac{2Ec_g}{c} \right) R_w^2 \quad (48)$$

where  $c_g$  is the wave group velocity,  $c$  is the phase velocity,  $E = \frac{1}{2}\rho g A_i^2$  is the wave energy. The added mass and damping coefficients will be evaluated using Equation (44) and Equation (45), respectively. The exciting force coefficients will be addressed using Equation (41). The transmission and reflection coefficients could be evaluated using Equation (46) and Equation (47) for the analytical and Equation (48) for the numerical method.

### 3. RESULTS

Based on the formulation discussed in section 2, Equation 39 is solved in MATLAB<sup>®</sup> with inputs being  $\theta$ ,  $a$ ,  $b$ ,  $h_1$ ,  $h_2$ ,  $s_1$ ,  $d$ ,  $A_i$  and the number of truncated terms in the orthogonal series being  $N = 12$ .

The solution is the unknown coefficients in orthogonal series which determine the velocity potentials for the diffraction and radiation terms according to Equation (19)-(26). Hydrodynamic characteristics of the domain are then evaluated using Equation (40)-(47). In order to verify the analytical method, a rectangular SB of  $s_1/h_1 = 0.2$ ,  $a/h_1 = 0.2$ ,  $h_1/b = 6$ ,  $\theta = 30^\circ$  is considered. The model characteristic has been chosen

similar to Zheng et al. (2007) for validation purposes. Furthermore, a BEM numerical simulation using ANSYS AQWA is carried out for comparison. Figure 2 demonstrates the added mass coefficient ( $C_m$ ), the damping coefficients ( $C_d$ ), and the exciting force coefficients ( $CF$ ) of the proposed breakwater. These are compared with Zheng et al. (2007). Evidently, all results are in reasonable agreement. The divergence between numerical and analytical results are thought to originate from converting three-dimensional results to two-dimensional quantities in numerical simulation. It should be emphasized that in analytical solution, the length of the breakwater mathematically assumed to be infinite, however, in numerical simulation the length of the breakwater considered to be 50 m. Table (1) summarises the model characteristics of the geometry, environmental constants, mass properties and mesh parameters for the numerical model. It should be noted that de-featuring tolerance controls how small details are treated by the mesh in AQWA. If any detail in the structure is smaller than this tolerance, a single element may span over it, otherwise the mesh size will be reduced in this area to ensure that the feature is meshed. In AQWA the maximum element size is explicitly related to the maximum wave frequency that can be utilized in the diffraction analysis. If a particular maximum wave frequency is desired, this can be specified as *maximum allowed frequency* and the associated maximum element size will be computed. In this study, after testing a number of maximum element size, the nearest value to the desired frequency range ( $f_i \approx 0 - 0.4 \text{ Hz}$ ) is chosen. Desired frequency range is calculated according to the dispersion equation (Equation 5) with respect to the desired wave number which covers a range of response similar to Zheng et al. (2007). It should be emphasized that for the radiation term, according to Equation (44) and Equation (45),  $C_m$  and  $C_d$  are independent of incident wave amplitude. However for the diffraction term and for the evaluation of  $CF$ , according to Equation (41), it is assumed that  $A_i = 1m$ .

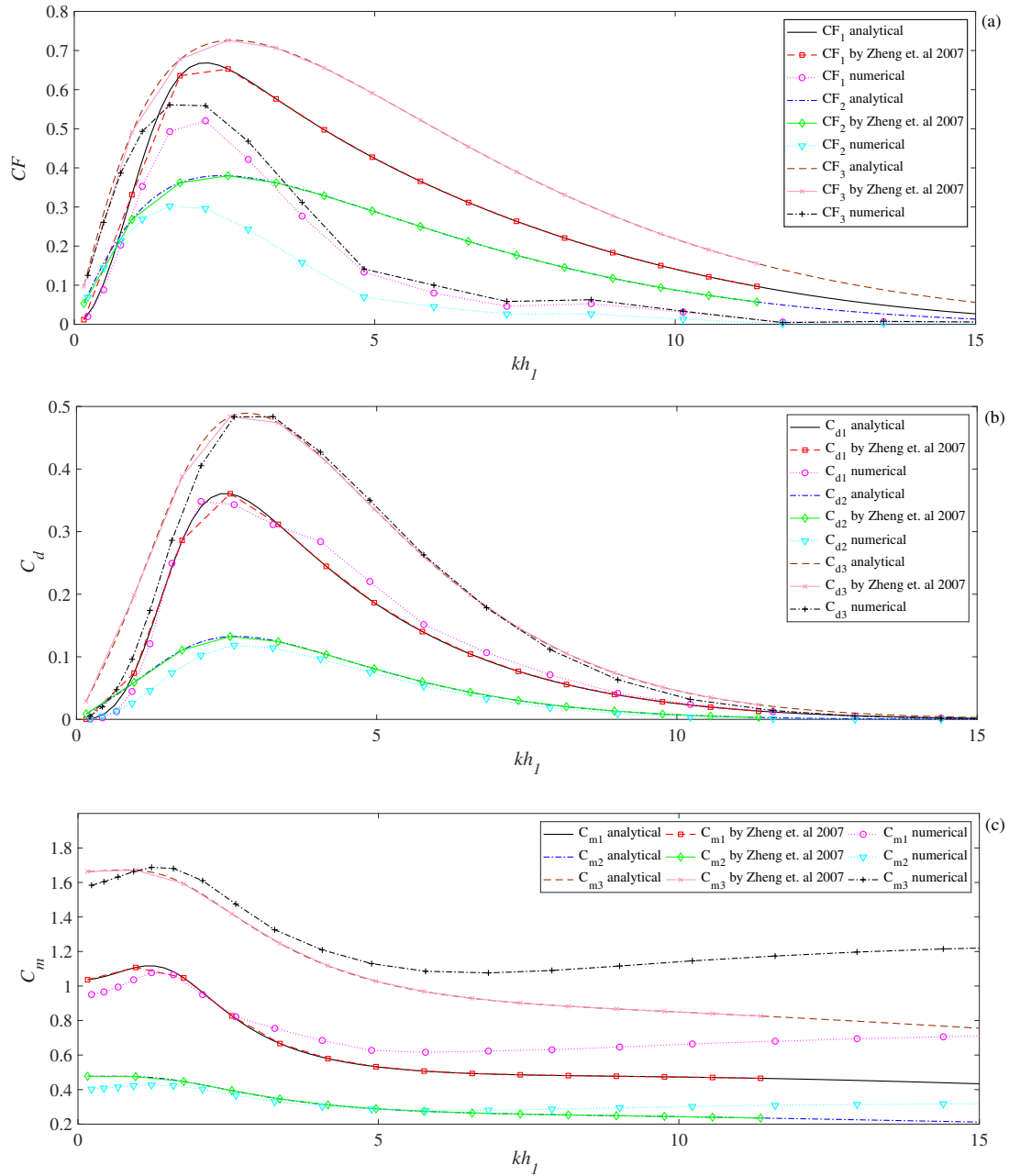


Figure 2: Comparison of numerical and analytical study on (a) exciting forces  $CF_u$  (b) damping coefficients  $C_{d_u}$  and (c) added mass coefficients  $C_{m_u}$  of heave ( $u = 1$ ), sway ( $u = 2$ ) and roll ( $u = 3$ ) motions/directions ( $s_1/h_1 = 0.2$ ,  $a/h_1 = 0.2$ ,  $h_1/b = 6$ ,  $\theta = 30^\circ$ )

#### 415 *Horizontal and Vertical Flat SBs*

416 Two types of high aspect ratio SBs are studied  
 417 in this work and their configurations are pre-  
 418 sented in Figure 3. The first one is denoted as a  
 419 horizontal flat breakwater and the second one as  
 420 vertical.

421 Figure 4 displays the exciting force coeffi-  
 422 cients, as defined in Equation (41), of horizon-

tal and vertical flat SBs at conditions  $s_1/h_1 =$  423  
 $0.1$ ,  $\theta = 1^\circ$ . In the present analytical method, 424  
 $\theta = 0^\circ$  is a singular condition, hence  $\theta = 1^\circ$  is con- 425  
 sidered instead. Analytical and numerical meth- 426  
 ods are depicted simultaneously and reasonable 427  
 agreement between the two is evident. 428

According to Equation (48), the mean drift 429  
 force on the body can be calculated. The trans- 430

Table 1: Breakwater specifications, environmental constants and mesh parameters for numerical simulation

Geometry		Environmental Constants	
Length ( $y$ )	50 m	Water Depth	48 m
Width ( $x$ )	16 m	Water Density	1025 kg/m <sup>3</sup>
Depth ( $z$ )	9.6 m	Gravity	9.8 m/s <sup>2</sup>
Mass Properties		Water Size $x$	1000 m
$x_0$	0 m	Water Size $y$	1000 m
$y_0$	0 m	Mesh Parameters	
$z_0$	-14.4 m	De-featuring Tolerance	1 m
Mass	15744 t	Maximum Element Size	2 m
$K_{xx}$	29 m	Maximum Allowed Frequency	0.431 Hz
$K_{yy}$	5.4 m	Total Nodes	3922
$K_{zz}$	29.2 m	Total Elements	3920

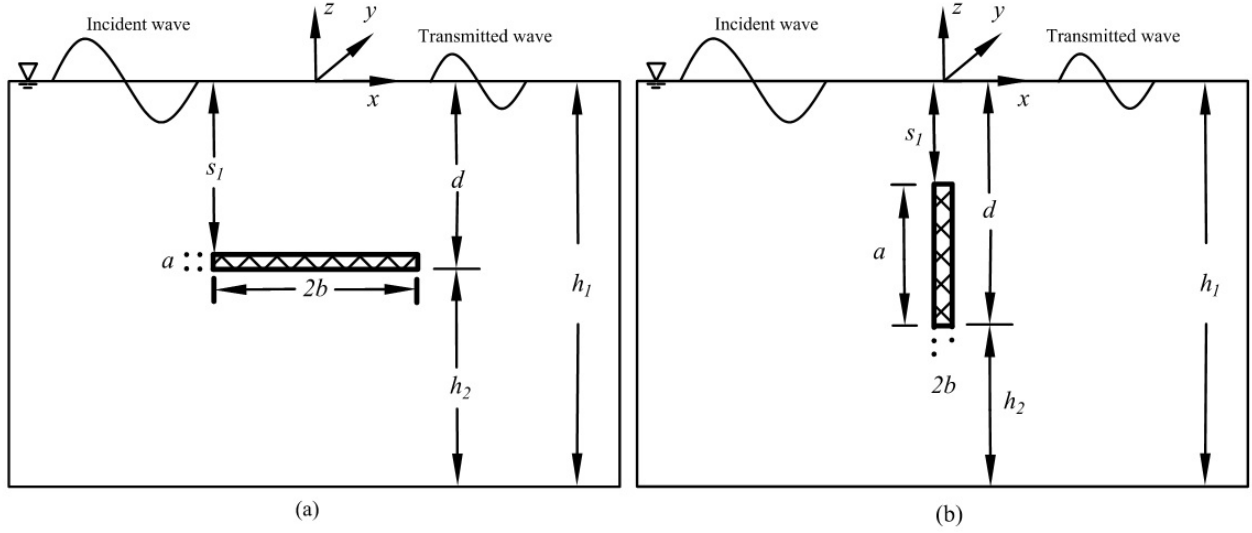


Figure 3: Basic configuration and coordinate system for (a) horizontal and (b) vertical flat SBs

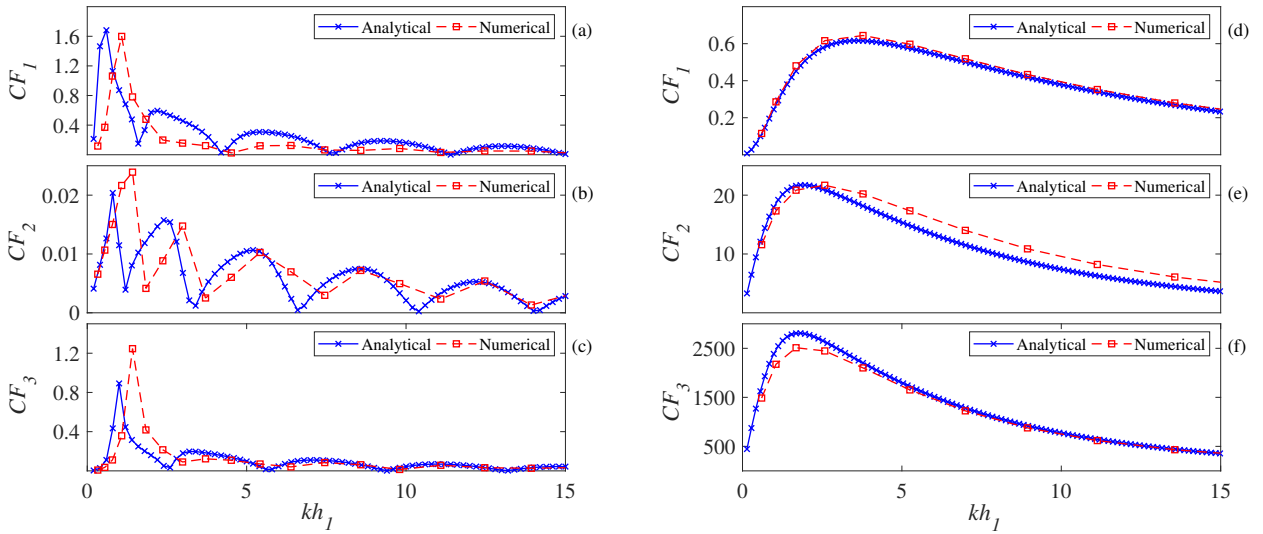


Figure 4: Exciting force coefficients for horizontal (a,b,c) and vertical (d,e,f) flat SBs ( $s_1/h_1 = 0.1$ ,  $\theta = 1^\circ$ )

431 mission and reflection coefficients can then be  
 432 derived and the results are shown in Figure 5  
 433 for the vertical and the horizontal flat SBs of  
 434  $s_1/h_1 = 0.1$ ,  $\theta = 1^\circ$ . It should be noted that  
 435 for the cases under consideration in Figure 3, the  
 436 horizontal flat SB has a ratio  $2a/b = 100$  and for  
 437 the vertical flat SB,  $2a/b = 0.01$ .

#### 438 4. DISCUSSION

439 Figure 4 shows that exciting force coefficient  
 440  $CF$ , which represents the combined effect of the  
 441 incident and diffraction forces, oscillates as a func-  
 442 tion of wave number. Exciting forces for the  
 443 horizontal flat breakwater are shown in Figure 4  
 444 (a,b,c) and that for the vertical flat breakwater  
 445 are shown in Figure 4 (d,e,f). For the horizontal  
 446 flat breakwater (a,b,c), exciting force coefficient  
 447 varies both globally and locally with respect to  
 448 the dimensionless wave number ( $kh_1$ ). Globally,  
 449 as the incident wave frequency increases, the force  
 450 decreases quickly. Local oscillation can also be  
 451 seen. It causes  $CF_u$  to drop to zero at multiple  
 452 wave numbers with an appeared phase lag from  
 453  $CF_1$  to  $CF_3$ . For large wave numbers,  $CF_u$   
 454 approaches to zero globally. The exciting force coef-  
 455 ficient of the sway motion,  $CF_2$ , is much smaller  
 456 in magnitude than  $CF_1$  (heave) and  $CF_3$  (roll).  
 457 Note the different ordinate scales. Physically this  
 458 is owing to the smaller projected area in the sway  
 459 direction for the horizontal flat breakwater. Dis-  
 460 crepancies between analytical and numerical re-  
 461 sults can be observed, which could be a result  
 462 of converting three-dimensional analysis to two-  
 463 dimensional quantities in numerical method.

464 The behaviour of the exciting force associated  
 465 with the vertical flat breakwater (d,e,f) appears  
 466 to be very different. Although they also display  
 467 a global decay as  $kh_1$  increases, no local oscilla-  
 468 tion is observed. This is believed to be due to  
 469 diffraction force, which is mainly responsible for  
 470 the oscillatory force behaviour, having negligible  
 471 magnitude. The very large exciting force coeffi-  
 472 cient of the roll motion,  $CF_3$ , is related to the  
 473 large projected area of the breakwater in the roll  
 474 direction. It thus suggests that the vertical geom-  
 475 etry has a high tendency to roll.

476 Figure 5 demonstrates transmission and reflec-  
 477 tion coefficients for both horizontal flat and ver-  
 478 tical flat breakwaters using numerical method. It  
 479 can be seen from the behaviour of  $T_w$  and  $R_w$  that  
 480 the vertical flat breakwater almost transmits the  
 481 entire incident wave energy (no reflects). On the  
 482 contrary, the horizontal flat breakwater effectively  
 483 attenuates incident wave energy especially for low  
 484 wave numbers over the range  $1 < kh_1 < 3$ , in  
 485 which transmission coefficient  $T_w$  reaches the min-  
 486 imum value  $\approx 0.4$  and  $R_w$  reaches the maximum  
 487 value of  $\approx 0.84$ . Those are considerable values  
 488 comparing to conventional low aspect ratio SB.

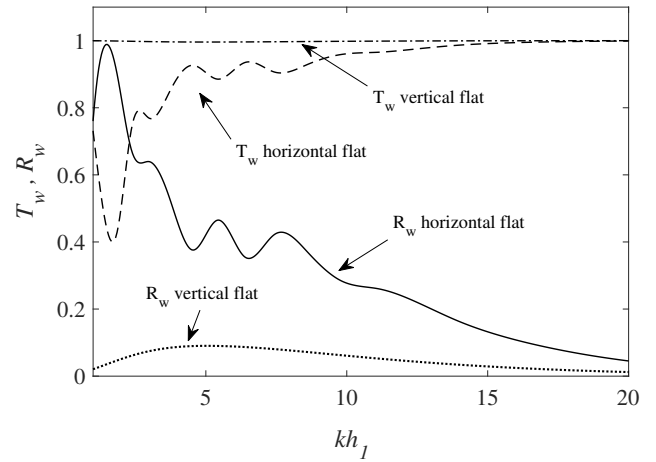


Figure 5: Transmission and reflection coefficient compari-  
 son of horizontal and vertical flat SBs ( $s_1/h_1 = 0.1$ ,  $\theta = 0$ )

489 An oscillatory behaviour can also be seen  
 490 for  $T_w$  and  $R_w$  for the horizontal flat breakwa-  
 491 ter, which is a direct reflection of the oscillatory  
 492 diffraction force shown in Figure 4 (a,b,c). Addi-  
 493 tionally, no oscillatory behaviour is observed for  
 494 vertical flat breakwater's  $T_w$  and  $R_w$ , which is in  
 495 consistence with the exciting force in Figure 4  
 496 (d,e,f). It is plausible that diffraction wave forma-  
 497 tion on the vertical and the horizontal flat break-  
 498 water is the basic reason for the large difference  
 499 in their transmission coefficient behaviours. The  
 500 large size in the  $x$  direction of the horizontal flat  
 501 breakwater leads to a lower transmission coeffi-  
 502 cient, as has been the main parameter in many  
 503 previous FB studies. Additionally, it suggests  
 504 that the breakwater's dimension in the incident  
 505 wavelength direction plays the dominant role in

506 the performance of SBs as well as FBs.  
507 In order to determine the effect of submer-  
508 gence depth on the reflection and transmission  
509 coefficients of the horizontal flat SB, Figure 6 is  
510 presented. First of all, as  $s_1/h_1$  increases, the re-  
511 flection coefficient  $R_w$  decreases and the transmis-  
512 sion coefficient  $T_w$  increases. For  $s_1/h_1 = 0.2$  the  
513  $T_w$  reaches a minimum value of 0.75 at  $kh_1 \approx 2.5$ ,  
514 which means 75% of incident wave energy is trans-  
515 mitted from the breakwater. Secondly, as it can  
516 be seen, the weak oscillatory behaviour vanishes  
517 as  $s_1/h_1$  increases, which suggests that the oscil-  
518 latory behaviour in diffraction problem of SBs,  
519 especially for horizontal flat, increases as the sub-  
520 mergence depth decreases. The physical explana-  
521 tion of this behaviour might relate to the diffrac-  
522 tion wave height. As the height increases with  
523 decreasing submergence depth, for low enough  $s_1$ ,  
524 the body is influenced (or partially influenced)  
525 by its own diffraction wave. Because the diffrac-  
526 tion wave formation is an oscillatory function of  
527  $\exp(ix)$ , it reflects itself in  $CF$ ,  $T_w$  and  $R_w$ . How-  
528 ever, when  $s_1$  is large enough, the body and the  
529 produced diffraction wave will not collapse and  
530 parameters like  $CF$ ,  $T_w$  and  $R_w$  do not show os-  
531 cillatory trends.

532 Figure 7 shows the formation of the diffrac-  
533 tion wave amplitude  $A_d$  alongside the breakwa-  
534 ter's width on the horizontal flat breakwater for  
535  $\theta = 0^\circ$  and  $s_1/h_1 = 0.1$  using numerical method.  
536 Firstly,  $A_d$  increase with  $2b/h_1$ . Such an increase  
537 is much more appreciable in (a) and (b), com-  
538 pared to (c) and (d). Secondly, diffraction wave  
539 length decreases quickly with increasing breakwa-  
540 ter width  $b$ .

541 Figure 8 shows the dependence of the maxi-  
542 mum diffraction wave amplitude  $|A_{d_{max}}|$  on the  
543 submergence depth  $s_1$  and breakwater's width  $2b$ .  
544 According to Figure 7,  $|A_{d_{max}}|$  occurs at  $x = b$   
545 where  $A_d$  start to decrease afterwards.  $|A_{d_{max}}|$   
546 is normalised by the amplitude of the incident  
547 wave  $A_i$ . Figure 8 (a,b,c) present the results  
548 from the incident wave's frequency  $f_i = \omega/2\pi$   
549 of  $0.2 Hz$ ,  $0.15 Hz$  and  $0.11 Hz$ , respectively,  
550 and the curves in each subfigure are different by  
551 changing the values of  $s_1/h_1$ . It can be seen  
552 that at fixed  $s_1/h_1$ , increasing  $2b/h_1$  (breakwater's

width) results in a smooth increase in  $|A_{d_{max}}|/A_i$  553  
for all incident wave frequencies. On the other 554  
hand, at fixed  $2b/h_1$ , as  $s_1/h_1$  (the submergence 555  
depth) decreases,  $|A_{d_{max}}|/A_i$  increases and the in- 556  
crement rate diminishes quickly from  $f_i = 0.2Hz$  557  
to  $0.11Hz$ . Actually, all of  $s_1/h_1$  trends, almost 558  
collapse each other in  $f_i = 0.11 Hz$ . It perhaps 559  
can be expected that at very low incident wave 560  
frequencies, the curves would become flat and the 561  
amplitude  $|A_{d_{max}}|$  would be independent of  $s_1/h_1$ . 562

Figure 8 (d,e,f) show the dependence of 563  
 $|A_{d_{max}}|/A_i$  on  $s_1/2b$ . Firstly, it can be seen clearly 564  
that for a given value of  $s_1/2b$ , increasing  $2b/h_1$ , 565  
i.e. decreasing the overall water depth, would 566  
lead to diminishing  $|A_{d_{max}}|/A_i$ . Secondly, it is 567  
observed, especially in (e) and (f), that as  $s_1/2b$  568  
decreases to very low values, i.e. for very low 569  
submergence depth, the normalised diffraction 570  
wave amplitude  $|A_{d_{max}}|/A_i$  tends to converge to a 571  
specific value  $\approx 3.0$ , regardless of the  $2b/h_1$  value, 572  
i.e. regardless of the overall water depth at least 573  
for the range tested. Physically, the converged 574  
 $|A_{d_{max}}|/A_i$  value infers zero transmission coeffi- 575  
cient in which all incident wave energy is reflected 576  
due to high amplitudes of diffraction waves and 577  
after this point, according to the conservation of 578  
energy law, increasing the breakwater's width (or 579  
decreasing the parameter  $s_1/2b$ ) would not results 580  
in an increase in diffraction wave amplitude any 581  
more. This result, perhaps surprisingly, shows 582  
that even for SBs, if the geometric characteristics 583  
of the body is appropriate, zero transmission 584  
coefficient can be achieved. Furthermore, the 585  
convergent value ( $\approx 3.0$ ) seems to be independ- 586  
ent of the incident wave frequency. It should 587  
be noted that because of the shortcomings of the 588  
numerical method, some results in low  $s_1/2b$  was 589  
not achievable (especially for Figure 8 (d)), how- 590  
ever, the global trends show foreseeable order, 591  
reaching the convergent value of  $|A_{d_{max}}|/A_i \approx 3$ . 592

## 5. CONCLUSIONS 593

In this study two-dimensional SBs with rect- 594  
angular cross section in finite water depth in reg- 595  
ular waves are studied and verified for further im- 596  
plementation. Two new breakwaters, horizontal 597

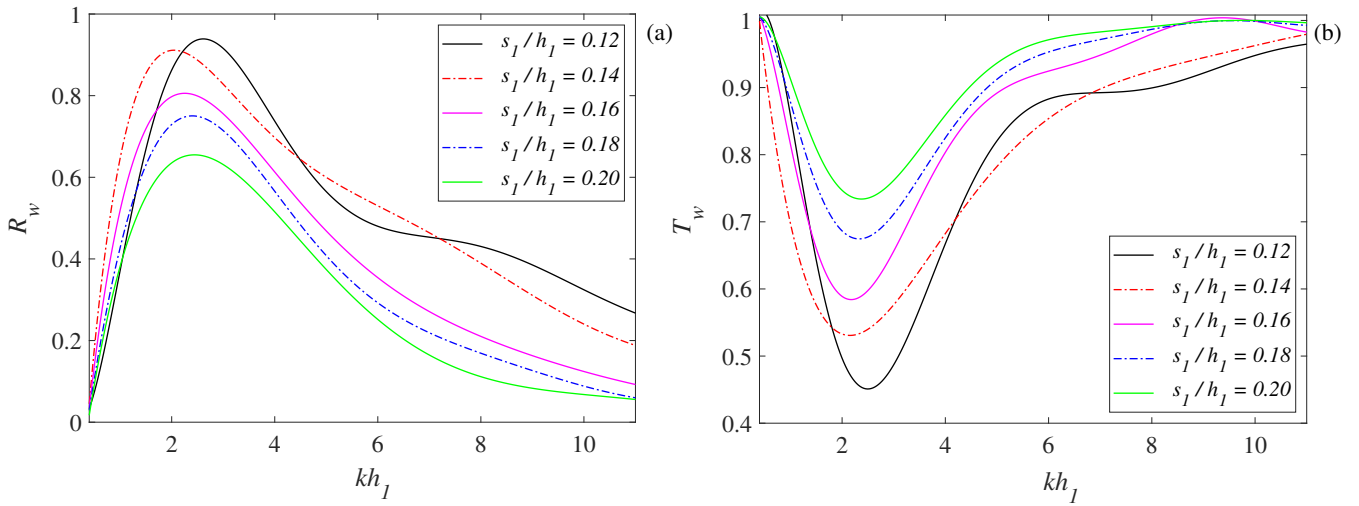


Figure 6: Reflection and transmission coefficients of horizontal flat SB in different submergence depths  $\theta = 0$

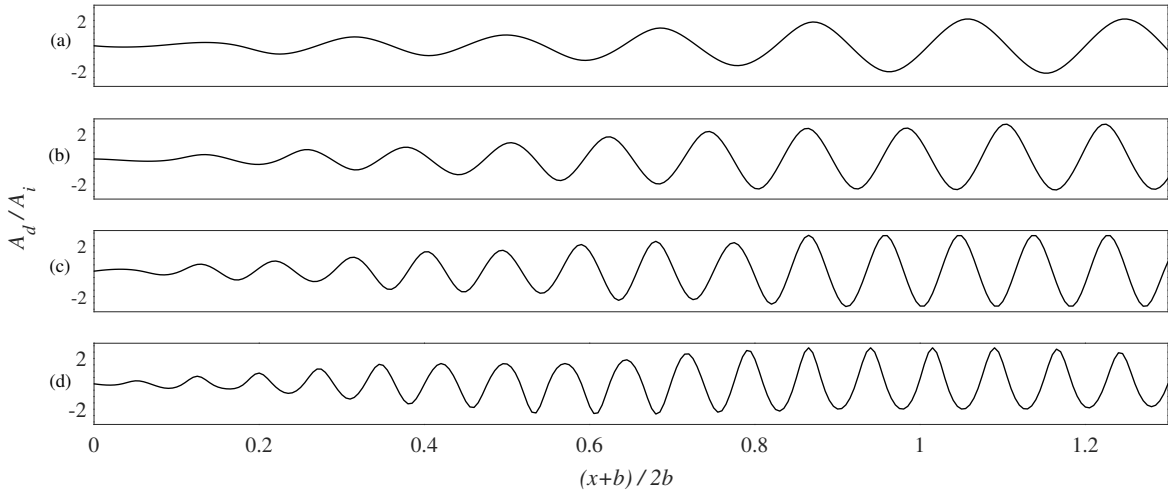


Figure 7: None-dimensional diffraction wave amplitude of horizontal flat breakwater ( $\theta = 0^\circ$ ,  $s_1/h_1 = 0.1$ ) for (a)  $2b/h_1 = 2$ , (b)  $2b/h_1 = 3$ , (c)  $2b/h_1 = 4$ , and (d)  $2b/h_1 = 5$  all in  $f_i = 0.2Hz$

598 and vertical flat SBs of high aspect ratio, are proposed  
 599 and their hydrodynamic characteristics are studied by the analytical and numerical methods.  
 600 Furthermore a parametric study on the diffraction wave amplitude, which is the dominant basic parameter  
 601 in breakwater's transmission coefficient, is carried out. The following conclusions can be drawn from this study:  
 602  
 603  
 604  
 605

- 606 • It is shown that the vertical flat SB produces almost no diffraction wave and transmits most of the incident wave energy. On  
 607 the other hand, the horizontal flat SB shows

610 relatively low transmission capability, which is desirable for many practical applications.  
 611

- 612 • The horizontal flat SB may be applied as an alternative to the existing breakwaters such as conventional submerged or floating  
 613 breakwaters, subjected to the consideration of construction, installation and maintenance factors etc.  
 614  
 615  
 616  
 617
- 618 • Diffraction wave formation associated with the two-dimensional rectangular SBs is a decaying or a growing function of  $x$ ,  $\exp(\pm jx)$ ,  
 619  
 620

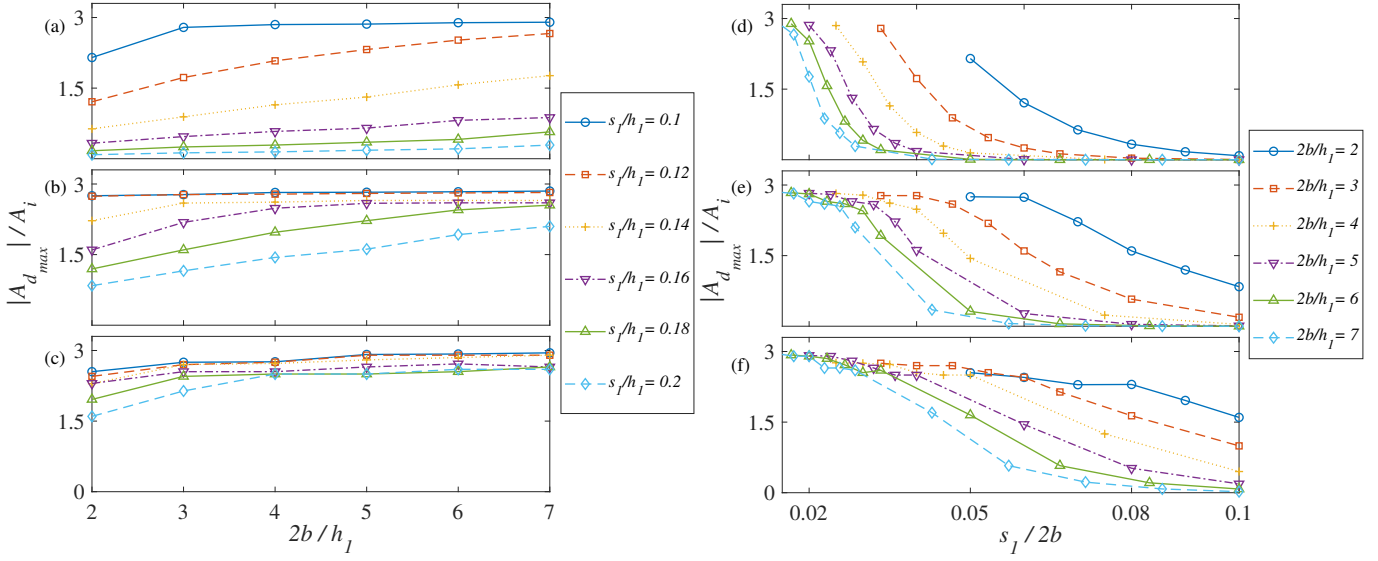


Figure 8: None-dimensional absolute maximum diffraction wave amplitude of horizontal flat breakwater ( $\theta = 0^\circ$ ) for  $f_i = 0.2Hz$  (a,d),  $f_i = 0.15Hz$  (b,e) and  $f_i = 0.11Hz$  (c,f)

621 which reaches the maximum value at free surface and on one of the edges of the breakwater, depending on the incident wave direction. Additionally, larger breakwaters (breakwaters with high aspect ratios in the direction of incident wave) produce smaller diffraction wavelengths for a given incident wave frequency.

- 629 • Diffraction wave amplitudes tend to converge to a specific value at small submergence depth to total width ratio. This maximum amplitude corresponds to zero transmission coefficient and shows that SBs at appropriate circumstances can reflect all incident wave energy. Also, this maximum amplitude occurs at  $x = b$  for  $\theta = 0$  and  $x = -b$  for  $\theta = 180$  and seems to be independent of the incident wave frequency.

### 639 Nomenclature

640	$\alpha_n$	eigenvalue of region IV
641	$\beta_n$	eigenvalue of region II
642	$\gamma_n$	eigenvalue of region I and III
643	$\lambda_n$	eigenvalue of region I and III

$\mu_n$	eigenvalue of region II	644
$\omega$	Incident wave circular frequency	645
$\rho$	Water density	646
$\theta$	Incident wave angle to $+x$ axis	647
$\nu_n$	eigenvalue of region IV	648
$\varphi_d$	Diffraction potential	649
$\varphi_i$	Incident wave potential	650
$\varphi_t$	Total potential	651
$\varphi_{r_{2p}}^L$	Particular potential for $L^{th}$ radiation motions in region II	652 653
$\varphi_{r_{4p}}^L$	Particular potential for $L^{th}$ radiation motions in region IV	654 655
$\varphi_r^L$	Radiation potential of the $L^{th}$ motion	656
$a$	Breakwater height	657
$A_d$	Diffraction wave amplitude	658
$A_i$	Incident wave amplitude	659
$A_{d_{max}}$	Maximum diffraction wave amplitude	660



- 732 Hulme, A., 1982. The wave forces acting on a float- 788  
733 ing hemisphere undergoing forced periodic oscillations. 789  
734 Journal of Fluid Mechanics 121, 443–463. 790
- 735 Kunisu, H., 2010. Evaluation of wave force acting on sub- 791  
736 merged floating tunnels. Procedia Engineering 4, 99– 792  
737 105. 793
- 738 Lee, J.F., 1995. On the heave radiation of a rectangular 794  
739 structure. Ocean Engineering 22, 19–34. 795
- 740 Li, B., Lau, S., Ng, C., 1991. Second order wave diffraction 796  
741 forces and run-up by finite—infinite element method. 797  
742 Applied ocean research 13, 270–286.
- 743 Longuet-Higgins, M.S., 1977. The mean forces exerted by  
744 waves on floating or submerged bodies with applications  
745 to sand bars and wave power machines. Proceedings  
746 of the Royal Society of London. A. Mathematical and  
747 Physical Sciences 352, 463–480.
- 748 Masoudi, E., 2019. Hydrodynamic characteristics of in-  
749 verse t-type floating breakwaters. International Journal  
750 of Maritime Technology 11, 13–20.
- 751 Masoudi, E., Zeraatgar, H., 2016. Application of method  
752 of separation of variables for analyzing floating break-  
753 water. Journal of Marine Engineering 11, 61–73.
- 754 Mohapatra, S., Soares, C.G., 2019. Interaction of ocean  
755 waves with floating and submerged horizontal flexible  
756 structures in three-dimensions. Applied Ocean Research  
757 83, 136–154.
- 758 Sannasiraj, S., Sundar, V., Sundaravadivelu, R., 1995. The  
759 hydrodynamic behaviour of long floating structures in  
760 directional seas. Applied Ocean Research 17, 233–243.
- 761 Sannasiraj, S., Sundaravadivelu, R., Sundar, V., 2001.  
762 Diffraction–radiation of multiple floating structures in  
763 directional waves. Ocean Engineering 28, 201–234.
- 764 Tabatabaei, S.M.R., Zeraatgar, H., 2018. Parametric com-  
765 parison of rectangular and circular pontoons perfor-  
766 mance as floating breakwater numerically. Polish Mar-  
767 itime Research 25, 94–103.
- 768 Williams, A., Lee, H., Huang, Z., 2000. Floating pontoon  
769 breakwaters. Ocean Engineering 27, 221–240.
- 770 Wu, G., 1993. Second-order wave radiation by a sub-  
771 merged horizontal circular cylinder. Applied Ocean Re-  
772 search 15, 293 – 303.
- 773 Wu, G., Taylor, R.E., 1990. The second order diffraction  
774 force on a horizontal cylinder in finite water depth. Ap-  
775 plied Ocean Research 12, 106 – 111.
- 776 Wu, G., Taylor, R.E., 2003. The coupled finite element  
777 and boundary element analysis of nonlinear interactions  
778 between waves and bodies. Ocean Engineering 30, 387–  
779 400.
- 780 Yamamoto, T., Yoshida, A., Ijima, T., 1980. Dynamics  
781 of elastically moored floating objects. Applied ocean  
782 research 2, 85–92.
- 783 Zhan, J.m., Chen, X.b., Gong, Y.j., Hu, W.q., 2017.  
784 Numerical investigation of the interaction between  
785 an inverse t-type fixed/floating breakwater and regu-  
786 lar/irregular waves. Ocean engineering 137, 110–119.
- 787 Zheng, Y., Liu, P., Shen, Y., Wu, B., Sheng, S., 2007.  
On the radiation and diffraction of linear water waves 788  
by an infinitely long rectangular structure submerged 789  
in oblique seas. Ocean engineering 34, 436–450. 790  
Zheng, Y., Shen, Y., You, Y., Wu, B., Jie, D., 2004b. On 791  
the radiation and diffraction of water waves by a rect- 792  
angular structure with a sidewall. Ocean Engineering 793  
31, 2087–2104. 794  
Zheng, Y., You, Y., Shen, Y., 2004a. On the radiation and 795  
diffraction of water waves by a rectangular buoy. Ocean 796  
engineering 31, 1063–1082. 797